IEEE Access
Multidisciplinary ⋮ Rapid Review ⋮ Open Access Journal

Received 5 September 2022, accepted 18 September 2022, date of publication 28 September 2022, date of current version 5 October 2022.

Digital Object Identifier 10.1109/ACCESS.2022.3209179

RESEARCH ARTICLE

Determination of Oil Pollutants by Microchannel Laser Induced Fluorescence Technology

PENGFEI CHENG[1], YANPING ZHU[2], CHUANJIN CUI[2], AND JINYAN PAN[1]
[1]School of Electrical and Control Engineering, Xuzhou University of Technology, Xuzhou 221018, China
[2]College of Electrical Engineering, North China University of Science and Technology, Tangshan, Hebei 063210, China

Corresponding author: Chuanjin Cui (cuichuanjin@163.com)

This work was supported in part by the National Natural Science Foundation of China under Grant 61771419 and Grant 21807034; and in part by the Natural Science Foundation of Hebei Province of China under Grant F2019209323, Grant F2019209443, and Grant F2019209599.

ABSTRACT Laser-induced fluorescence technology is an effective method for detecting oil pollutants. The laser induced fluorescence detection system was developed, and four parallel microchannel sample pools were designed to improve the detection accuracy of fluorescence signals. The grating scanning system is improved by introducing grating feedback link to improve the wavelength scanning accuracy of the system.The experimental results show that the wavelength scanning resolution of the microchannel laser-induced fluorescence detection system is improved by 0.4 nm. Aiming at the defects of the traditional parallel factor algorithm which is sensitive to the sample components, slow operation speed and easy to fall into local convergence, the generalized inverse singular value decomposition is used to improve the parallel factor algorithm. Configure different concentrations of diesel, gasoline and kerosene solution samples. The experimental verification shows that the excitation-emission spectra of each component obtained by the improved parallel factor algorithm are highly consistent with the measured spectral characteristics, indicating that the microchannel laser-induced fluorescence detection system combined with the improved parallel factor analysis method can accurately identify oil pollutants.

INDEX TERMS Petroleum pollutants, three dimensional fluorescence spectrum, optical path of fluorescence detection, micro sample cell, parallel factor analysis.

I. INTRODUCTION

Oil pollution is a serious threat to the natural environment and human health. Therefore, the identification and treatment of oil pollution is very important. Petroleum-based substances are composed of aromatic hydrocarbon components and their derivatives with strong fluorescent properties, and the components are complex, and the components and contents of different types of oil are different. The detection methods of petroleum mainly include infrared spectroscopy, gas chromatography and fluorescence spectroscopy. Among them, fluorescence analysis technology can obtain more fluorescence information and has the advantages of high accuracy and good selectivity, so it is widely used in the field of oil identification [1], [2], [3], [4], [5], [6].

The associate editor coordinating the review of this manuscript and approving it for publication was Norbert Herencsar.

Laser-induced fluorescence (LIF) technology belongs to an emerging material component analysis technology in the discipline of analytical chemistry [7], [8], [9]. Compared with other spectral techniques, LIF has the following advantages: LIF is a zero background spectral technique with high sensitivity (up to $10^{-12} - 10^{-9}$ M, 5-6 orders of magnitude lower than UV-IR absorption method) [10], [11]. Fluorescence emission is omnidirectional and can be collected from various angles[12]. Due to the large size of the sample cell and low degree of automation of the conventional LIF detection system, microfluidic, as a miniaturized, integrated, high-throughput and low-cost analysis technology [13], [14], [15], can well solve these problems, and has been widely used in chemistry, biology, medicine, agricultural engineering and other related fields. Kim *et al.* [16] studied a fully automated disposable smart microfluidic platform (DIS-μChip). On-chip microfluidic flow sensors are

integrated with the platform and placed at all inlet and outlet channels, hereby allowing the DIS-μChip to be fully automated with a pressure control system. Owing to the film-chip technique, the superstrate was disposable and could prevent biological cross-contamination, which cannot be realized with conventional flow sensors. Li *et al.* [17] developed a simple, sensitive, instrument-free, CRISPR-based diagnostics of SARS-CoV-2 using a self-contained microfluidic system, achieving excellent sensitivity (94.1%), specificity (100%), accuracy (95.8%) and improved detection efficiency. Li *et al.* [18] proposed a novel microfluidics volume optical monitoring system (MVOMS). Functional channels embedded with hollow cylindrical waveguide (HCW) are integrated in MVOMS, which is convenient to realize the real-time monitoring and manipulating microfluidic. On this basis, they designed an integrated light-driven microfluidic quantitative sampling system, which can sample a specific volume of microfluidic in microchips automatically and accurately. Zaremba *et al.* [19] present a novel microfluidic system and the small footprint of their system makes it easy to integrate with other structures of microfluidic networks, ensure superior precision, repeatability and flexibility in concentration setting. In this paper, the LIF detection method is closely combined with microfluidic technology, and a microchannel laser-induced fluorescence detection system is developed to achieve high-precision detection of oil pollutants.

The parallel factor analysis method in the second-order correction analysis is an effective three-dimensional fluorescence spectral data analysis method. For the measured organic pollutant samples, the three-dimensional fluorescence spectra of the samples are measured by LIF technology, and the three-dimensional fluorescence spectra data are obtained. The parallel factor analysis method is used to realize the quantitative analysis of different components in the samples [20]. Kong *et al.* [21] used three-dimensional fluorescence spectroscopy combined with parallel factor analysis algorithm and pattern recognition method to characterize and classify petroleum pollutants, and compared with the classification models constructed by K-Nearest Neighbor (KNN) algorithm, principal component discriminant analysis (PCA-LDA) algorithm and partial least squares discriminant analysis (PLS-DA) algorithm, the results showed that the recognition accuracy of the PLS-DA model has the best recognition accuracy, and a reliable method is proposed for effective detection of oil pollutants. Liu *et al.* [22] applied fluorescence excitation emission matrix–parallel factor (EEM-PARAFAC) analysis to characterize textile industry wastewater and trace its presence in water bodies. Two protein-like components (C1 and C2) were identified as the source-specific indicators of textile industry wastewater, which was further demonstrated by conducting high-performance size exclusion chromatography analysis. However, the parallel factor analysis must choose the correct group fraction to ensure high resolution accuracy, and the convergence rate is slow in the iterative process. Therefore, based on the trilinear decomposition theory, an improved parallel factor algorithm is proposed, and the generalized inverse singular value decomposition method is used to improve the parallel factor algorithm.

In order to improve the detection accuracy of oil pollutants, in terms of hardware structure design, four groups of microchannel sample pools with the same structure were designed by microfluidic technology to enhance the intensity of fluorescence signals. The grating scale feedback grating splitting system is improved, and the grating detection feedback circuit is added to improve the wavelength scanning resolution.After preprocessing such as denoising and scattering for the obtained spectral data, the improved parallel factor analysis method was used to analyze the three-dimensional fluorescence spectral data of the measured pollutants, ensuring the resolution of mixed pollutants.

II. THEORIES

A. THE RELATIONSHIP BETWEEN SOLUTION CONCENTRATION AND FLUORESCENCE INTENSITY

The fluorescence intensity and concentration of oil pollutants follow Lambert-Beer law [23]. Within a certain concentration range, the relative fluorescence intensity of fluorescent substances in the solution is shown in equation (1)

$$I_f = KY_F I_0(1 - e^{-\varepsilon cl}) \tag{1}$$

where, I_f is the relative fluorescence intensity, K is the Instrument constant, Y_F is the fluorescence quantum yield, I_0 is the excitation light intensity (cd), ε is the molar absor-ption coefficient of fluorescent substance molecules (L/mol.cm), c is the fluorescent substance concentration in solution (mol/L), l is the fluorescence cell thickness (cm).

When the fluorescent substance is at a very low concentration in the solution, that is, $\varepsilon cl \leq 0.05$. Formula (1) where $e^{-\varepsilon cl} \approx 1 - \varepsilon cl$ in parentheses, the relative fluorescence intensity I_f can be simplified as:

$$I_f = KY_F I_0 \varepsilon cl \tag{2}$$

It can be seen from Formula (2) that if the solution of the fluorescent substance is in a relatively dilute solution state, the fluorescence intensity generated by the fluorescent substance in the solution is proportional to the concentration of the fluorescent substance in the solution under the irradiation of light with a certain intensity and a certain frequency [24]. Accordingly, the quantitative analysis of oil pollutants can be carried out.

B. OVERALL STRUCTURE OF FLUORESCENCE SPECTRUM DETECTION SYSTEM

The composition diagram of the fluorescence spectrum detection system is shown in Figure 1.

The light emitted from the light source is converted into a certain wavelength excitation light through collimating system 1 and splitting system 1, which excites the fluorescence material in the sample cell to produce fluorescence. The fluorescence is collected by the collimation system 2, and the

fluorescence of a single wavelength is output after being split by the spectroscopic system 2. The photodetector converts the fluorescent signal into an electrical signal, and outputs the electrical signal into the analysis system for fluorescence spectrum analysis [25].

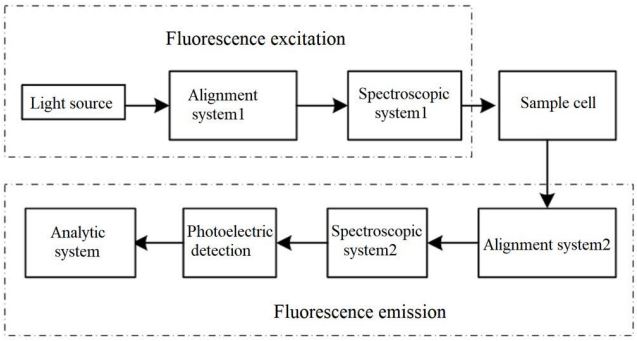

FIGURE 1. Structure diagram of fluorescence detection system.

C. IMPROVEMENT PRINCIPLE OF FOUR-CHANNEL FLUORESCENCE SPECTRUM DETECTION SYSTEM

In this paper, a multi-sample cell parallel structure is designed, the excitation light excites each sample to be tested, and the fluorescence generated by them is collected at the same time. The specific mechanism is shown in Figure 2.

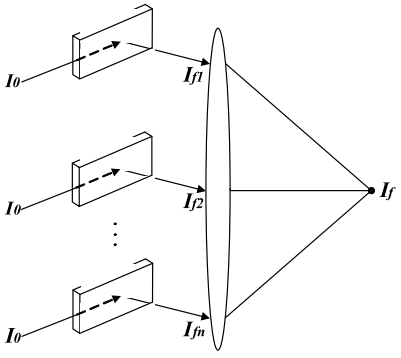

FIGURE 2. Schematic diagram of multiple sample cell.

The size of each sample cell in Figure 2 is the same, and the solution to be measured is the same. Where l is the solution transmitted light path, c is the concentration of the solution, ε is the absorption coefficient of the fluorescent substance in solution, I_0 is the incident light intensity, I_t is the transmitted light intensity, Y_F is the fluorescence quantum yield, The fluorescence intensity I_{fi} is proportional to $I_0 - I_t$ and fluorescence quantum yield Y_F is the same as (3).

$$I_{fi} = Y_F(I_0 - I_t) = Y_F I_0(1 - 10^{-\varepsilon cl}) \tag{3}$$

Expanding the exponential term in the above formula, the fluorescence emission intensity can be expressed as

$$I_{fi} = Y_F I_0(2.3\varepsilon cl - \frac{(2.3\varepsilon cl)^2}{2!} + \frac{(2.3\varepsilon cl)^3}{3!} - \cdots) \tag{4}$$

When the solution concentration is very thin, $\varepsilon cl \leq 0.05$, the higher order term in the formula can be omitted, and the fluorescence emission intensity I_{fi} increases with the increase of the molar concentration of the light absorbing material c, and it is linear. Then the formula (4) can be simplified to:

$$I_{fi} = 2.3Y_F I_0 \varepsilon cl \tag{5}$$

The (5) formula shows that the emission fluorescence intensity of the fluorescent material is related to the transmission path l of the excitation light in the sample cell.

Where, $i = 1, 2, \ldots, n$ is the number of parallel sample cells. Fluorescence focusing imaging of each sample cell. Then the total fluorescence intensity is the same as (6).

$$I_f = \sum_{i=1}^{n} I_{fi} = n2.3Y_F I_0 \varepsilon cl \tag{6}$$

The proportional relationship between fluorescence intensity and solution concentration in Eq. (2) is the theoretical basis for fluorescence quantitative analysis, but this linear relationship is the condition of $\varepsilon cl \leq 0.05$. In order to achieve this approximate linear condition, in the fluorescence analysis, the concentration c of the solution, the molar absorption coefficient ε of the solution and the transmission path l of the excitation light in the solution should not be too large. In this paper, changing the transmitted optical path l is taken as a breakthrough point to enhance the fluorescence intensity, but increasing the transmitted optical path l increases the nonlinearity between the fluorescence intensity and the solution concentration. Therefore, in this paper, four sample cells were designed for parallel excitation by microchannel processing technology to detect the fluorescence spectrum, and the fluorescence generated by them was collected. The transmitted light path of the excitation light of each sample satisfies an approximate linear relationship between the fluorescence intensity and the solution concentration. As shown in Eq. (6), when n is 4, the fluorescence intensity is correspondingly increased by 4 times. It can be seen that the sensitivity of the fluorescence detection system can be improved by parallel excitation of multiple sample cells.

III. IMPROVED MICROCHANNEL FLUORESCENCE SPECTROSCOPY DETECTION SYSTEM

The overall structure of the fluorescence spectrum detection system is shown in Figure 3. Spectral measurement range 250-600 nm. The wavelength resolution is 0.5 nm. Excitation and emission scanning step size range from 1-10nm. Four Parallel excitation sample cells are placed in the sample cell installation chamber.

A. DESIGN OF FOUR-CHANNEL SAMPLE CELL

Most of the detection cells of conventional fluorescence spectrophotometers use the standard quartz cuvette as the experimental sample container. Yuan *et al.* [26] used the excitation emission matrix fluorescence method to simultaneously determine the pesticide residues of carbendazim and

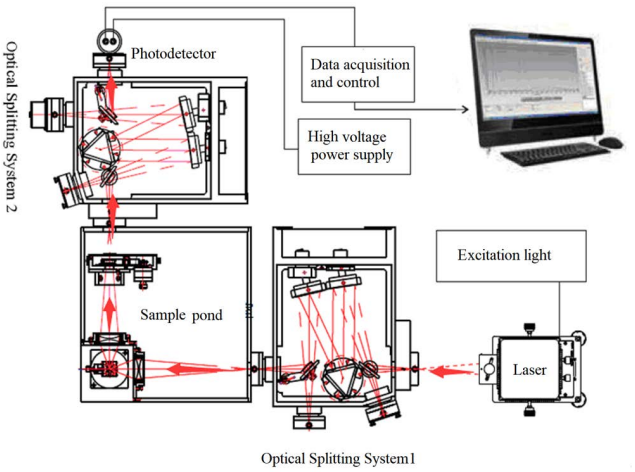

FIGURE 3. Structure of fluorescence spectrum detection system.

chlorothalonil in peanut oil. The sample cell of the FS920 fluorescence spectrum detection system was also a quartz cuvette. The size of the sample pool is large, the reagent consumption is large, and only manual sampling, the degree of automation is not high. The microchannel sample cell designed based on the mechanism of fluorescence detection is of great significance to realize the accurate detection of the measured object. Micromachining technology enables the miniaturization, integration, miniaturization and automation of products. At the same time, in order to increase the signal intensity, four groups of small sample pools with the same structure were used to realize the detection of petroleum pollutants.

The quartz glass parallel microchannel sample cell structure is adopted, is shown in Figure 4. The sample enters the microchannel from the in entrance, and when overflowing from the out entrance, it can be ensured that the sample is filled with the entire microchannel sample cell. The excitation light is divided into four beams I_0 by the spectroscopic system, and the four microchannel samples are excited respectively. After the emission spectrum If1 - If4 is aggregated, the total spectral signal is obtained. The parallel excitation of multiple microchannel samples can improve the fluorescence spectral signal intensity and the sensitivity of spectral signal detection.

Specified micro-channel structures were fabricated by femtosecond laser in quartz glass. The processing flow of the microfluidic sample cell is shown in Figure 5. Rotating coating on the surface of quartz glass substrate and the photographic plate printing is used to carve photoresist according to CAD drawings. The whole immersed tube pattern is displayed and dried. Finally, the sample system is formed by ion bonding on the quartz glass substrate. Microvalves are added at the liquid inlet of each injection system to control the liquid on and off. Femtosecond laser processing and modified quartz glass microchannels are porous and loose, which can be further corroded by hydrofluoric acid. The modified loose

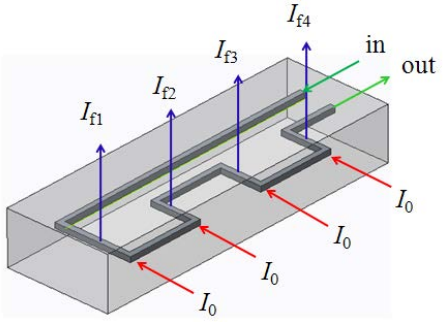

FIGURE 4. Quartz glass sample cell with parallel micro channel.

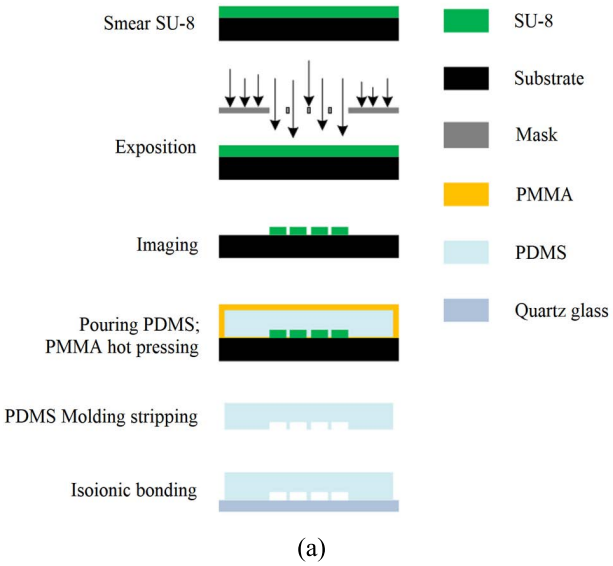

FIGURE 5. Micro-fluidic fabricate procedure diagram (a) microchannel processing flow diagram (b) microchannel ablated by femtosecond laser.

material is corroded and presents a complete microchannel. After calcination at 1000°C for 30 minutes, the surface inside the microchannel is smooth to achieve mirror effect. In order to solve the defect that the concentration of the microchannel system does not change quickly, a Christmas tree-shaped concentration gradient generator [27], [28] was used to explore the appropriate flow rate of microfluidics and form a good linear, stable and controllable concentration gradient.

Combined with the improved four-channel fluorescence spectrum detection system, the transient change of the concentration of oil pollutants are reliably reflected in the flow and measurement.

B. DESIGN OF GRATING SCATTERING AND SCANNING SYSTEM

The grating scanning system needs to split the 250-600nm complex light [29]. The sinusoidal mechanism is added to the grating spectrometer to improve the scanning resolution. The mechanism has the characteristics of high precision and reliability. The working principle of sine mechanism is shown in Figure 6. In Figure 6(a), the exit and entrance slits are fixed, and the light splitting process is realized by the rotation of the grating. In Figure 6(b), the dotted line B is the angular bisector of the angle between the incident light and the diffraction light, namely the initial position of the grating normal N. The dotted line N is the position of the grating normal after rotation. Angle ϕ is the angle of grating rotation. The initial incident angle of the excitation source is α, the diffraction angle is β, and the angle between the incident light and the diffraction light is δ.

The expression of diffraction wavelength λ and grating rotation angle is

$$\lambda = 2d\cos\frac{\delta}{2}\sin\varphi/m = (2d\cos i/m)\cdot\frac{h}{R} = k\cdot h \quad (7)$$

When the grating rotates around its center point, the angle δ is constant, and the grating constant d and coefficient $k = 2d\cos i/m$ are constant. It can be seen that the displacement of the screw slider is linear with the diffraction wavelength, that is, the wavelength of the monochromatic light can be known only by measuring the displacement of the slider.

In order to improve the wavelength scanning accuracy of the detection system, the grating feedback link is introduced, and the optical grating sensor is used to detect the slider displacement, and the detection results are fed back to the processor for data processing and analysis. The structure of grating splitting system is shown in Figure 7.

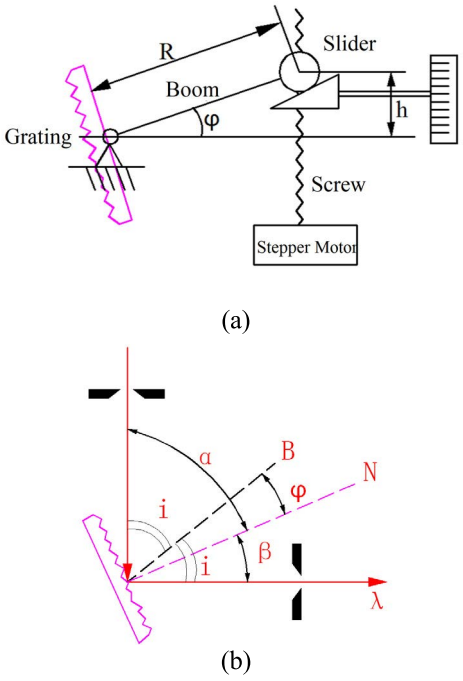

FIGURE 6. Diagram of sine screw scanning structure. (a) Sine screw scanning structure diagram. (b) Sine screw scanning principle diagram.

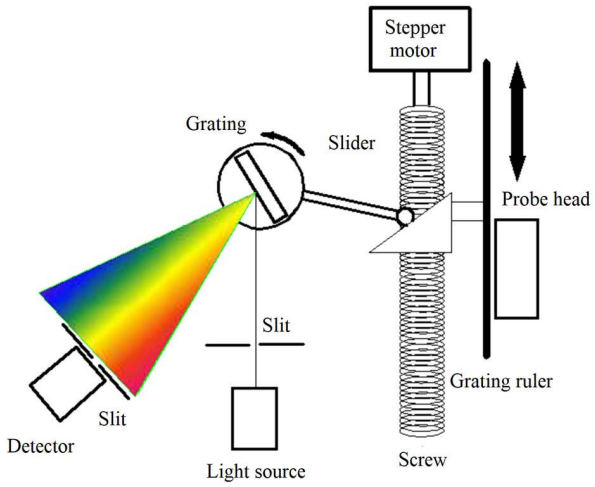

FIGURE 7. Structure diagram of the optical splitter.

IV. PARALLEL FACTOR ANALYSIS IMPROVEMENT

A. TRADITIONAL PARALLEL FACTOR ANALYSIS

Parallel factorization model decomposes a three dimensional matrix into three two dimensional matrices along three directions [30], As shown in Figure 8.

Based on the trilinear decomposition theory, each component of the three-dimensional matrix X is decomposed into score matrix A, loading matrix B and C by alternating least squares method with parallel factors. The decomposition model is:

$$x_{ijk} = \sum_{n=1}^{N} a_{in}b_{jn}c_{kn} + e_{ijk}$$
$$i = 1\ldots I, \quad j = 1\ldots J, \quad k = 1\ldots K \quad (8)$$

where, x_{ijk} is the X element, the fluorescence intensity of the i sample at emission wavelength j and excitation wavelength k, N is the factor number, that is, the total number of columns of the loading matrix, a_{in}, b_{jn}, and c_{kn} are the elements of matrix A, B, C. e_{ijk} is the elements of residual matrix E.

B. PARALLEL FACTOR ALGORITHM IMPROVEMENT

The traditional parallel factor analysis has the defects of slow convergence speed and too sensitive to the group fraction [31], [32], [33]. In order to avoid the above shortcomings of the parallel factor algorithm, the iterative process of the

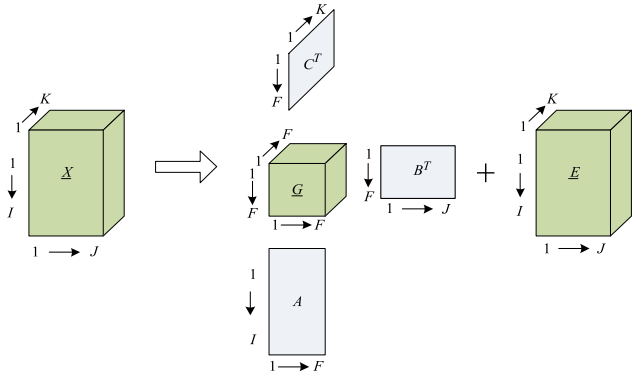

FIGURE 8. Three-dimensional measurement data matrix decomposed by PARAFAC.

parallel factor algorithm is improved by the principle of alternating least squares. The improvements are as follows:

1) Aiming at the iterative convergence process of the algorithm, the additive inverse singular value decomposition method in generalized inverse is adopted. Firstly, the iterative convergence error is set. When the singular value is less than the preset error value, it will be treated as 0. Even if the selected group fraction is greater than the actual group fraction, the results are not affected, It shows the robustness of the algorithm when there is interference to components.
2) Three closely related but not completely equivalent objective functions are established, and the three objective functions are iterated simultaneously. During the iterative process, if one objective function falls into the flat area of the iteration, the other two objective functions are not in the flat area, which speeds up the convergence.

The matrix form of the improved parallel factor algorithm model is:

$$X_{..k} = Adiag(c'_k)B^T + E_{..k}, \quad k = 1, 2, \cdots, K \tag{9}$$

where, $X_{..k}$ and $E_{..k}$ are the section k of X and E along the concentration direction, $\boldsymbol{A}$ and $\boldsymbol{B}$ are the Load matrix $A = (a_1, a_2, \cdots, a_N)$ and $B = (b_1, b_2, \cdots, b_N)$ obtained by decomposition, c_k is the Line k of matrix $C = (c_1, c_2, \cdots, c_N)$, $diag(c_k)$ are the c_k diagonal matrix with dimension $N \times N$ consisting of elements of line k in c_k, N is the number of factors used in trilinear decomposition.

The main idea of the parallel factor improvement algorithm is to obtain the load moment A, B, C by alternately optimizing the objective function $F(A, B, C)$.

$$F(A, B, C) = \sum_{k=1}^{K} \left\| X_{..k} - Adiag\left(c'_k\right) B^T \right\|_F^2 \tag{10}$$

According to the least squares principle (ALS) and the properties of the matrix, a new iterative derivation for A, B, C formula:

$$a_{(i)}^T = diag\left(CX_{i..}\left(B^+\right)^T\right), \quad i = 1, 2, \cdots, I$$

$$b_{(j)}^T = diag\left(AX_{.j.}\left(C^+\right)^T\right), \quad j = 1, 2, \cdots, J$$
$$c_{(k)}^T = diag\left(BX_{..k}\left(A^+\right)^T\right), \quad k = 1, 2, \cdots, K \tag{11}$$

where, $diag(\cdot)$ is the New vectors, the elements in the square matrix in parentheses, $a_{(i)}$, $b_{(j)}$ and $c_{(k)}$ are the row vector of relative concentration matrix A, relative fluorescence emission spectrum matrix B and relative fluorescence excitation spectrum matrix C, respectively.

The iterative process uses the three formulas in formula (9) to solve iteratively, and uses the alternating least square-s principle to repeatedly calculate $a_{(i)}$, $b_{(j)}$, $c_{(k)}$, so that the SSR value is less than the set 1×10^{-6}. The generalized inverse calculation method is applied to the PARAFAC algorithm, which improves the anti-interference ability of the preset tolerance difference and reduces the deviation of the predicted group score. The least square steps are simplified to obtain the ideal decomposition results effectively.

V. EXPERIMENT

A. COMPARATIVE EXPERIMENT ON WAVELENGTH RESOLUTION OF GRATING SCANNING SYSTEM

The experimental equipment used is: planar reflection blazed grating, HEIDENHAIN LC493M grating ruler, Sensor for measuring slider displacement, Stepper motor driving a sinusoidal screw, Ball screw with pitch of $1nm$(sinusoidal screw), After experimental measurement, the resolution of the selected grating ruler at $600nm$ is $0.0109nm$, which is much smaller than $0.12nm$ of the designed scanning system.

The three peak wavelengths of the high-pressure mercury lamp ($365nm$, $403nm$ and $546nm$) were used as the standards for the experimental test of the spectrometer. The wavelength test values are shown in Figure 9. It can be seen from Figure 9 that the wavelength scanning resolution of the grating rotation angle driven by the traditional stepper motor and the screw structure is $\pm 0.7nm$, while after the grating detection feedback circuit is added, the wavelength scanning resolution is $\pm 0.3nm$, which improves the wavelength scanning resolution.

B. EXPERIMENTAL RESEARCH ON MICROCHANNEL FLUORESCENCE SPECTROSCOPIC DETECTION SYSTEM

F-7000 fluorescence spectrophotometer and micro-channel fluorescence spectrum detection system were used to detect pure 0# diesel, gasoline CCl_4 standard solution and three kinds of oil mixed solutions (kerosene, gasoline, diesel concentration: 0.25mg/L, 0.25mg/L, 0.25mg/L) samples were tested. As shown in Figures 10, 11 and 12, the comparison shows that the fluorescence intensity signal measured by the microchannel fluorescence spectrum detection system is enhanced compared with the spectral signal measured by the F-7000 spectrophotometer.

C. EXPERIMENTAL STUDY ON THREE-DIMENSIONAL FLUORESCENCE SPECTROSCOPY OF PETROLEUM POLLUTANTS

Preparation of0#diesel, -10#diesel, 97#gasoline, 93#gasoline and kerosene concentration of 104 mg/L standard solution 1

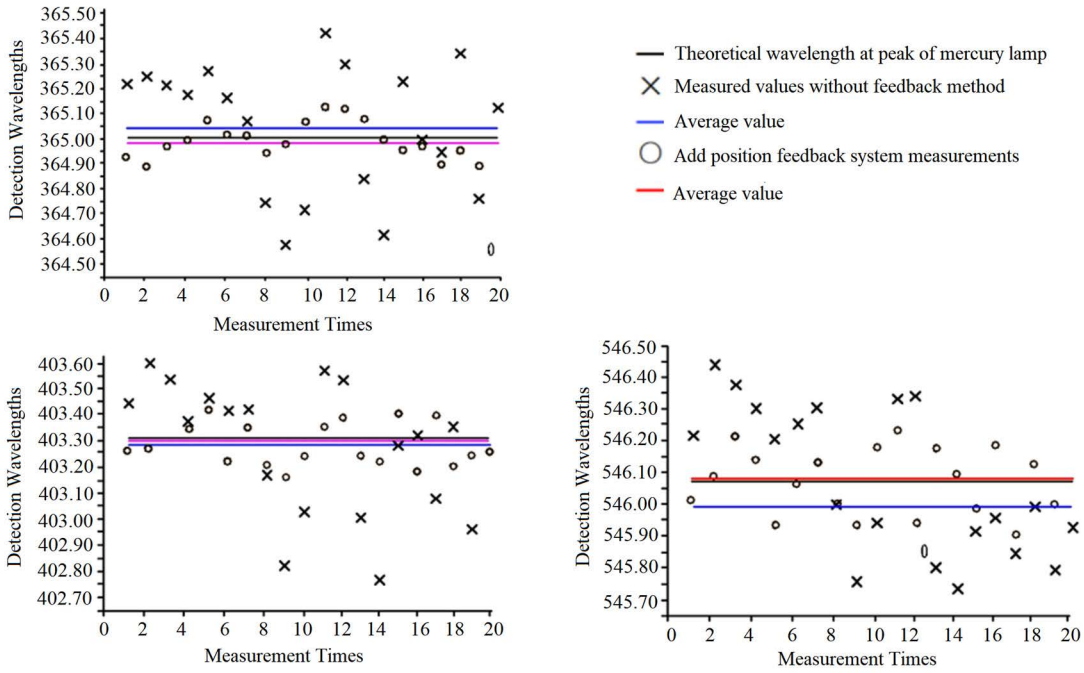

FIGURE 9. Test results at the peak of high-pressure mercury lamp.

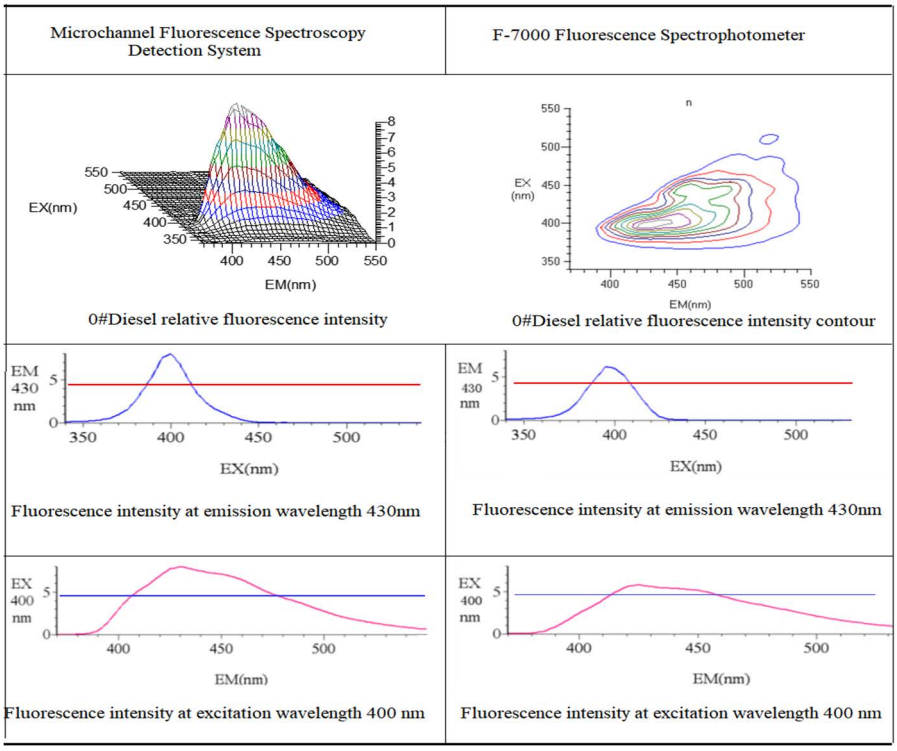

FIGURE 10. Fluorescence spectra of pure 0# diesel.

and concentration of 100mg/L standard solution 2 respectively. Three - component and four - component samples were prepared with different volume standard solution 1 or 2. Among the four components, the samples no. 1-6 samples were used as the calibration samples, and the samples no. 7-10 samples were used as the prediction

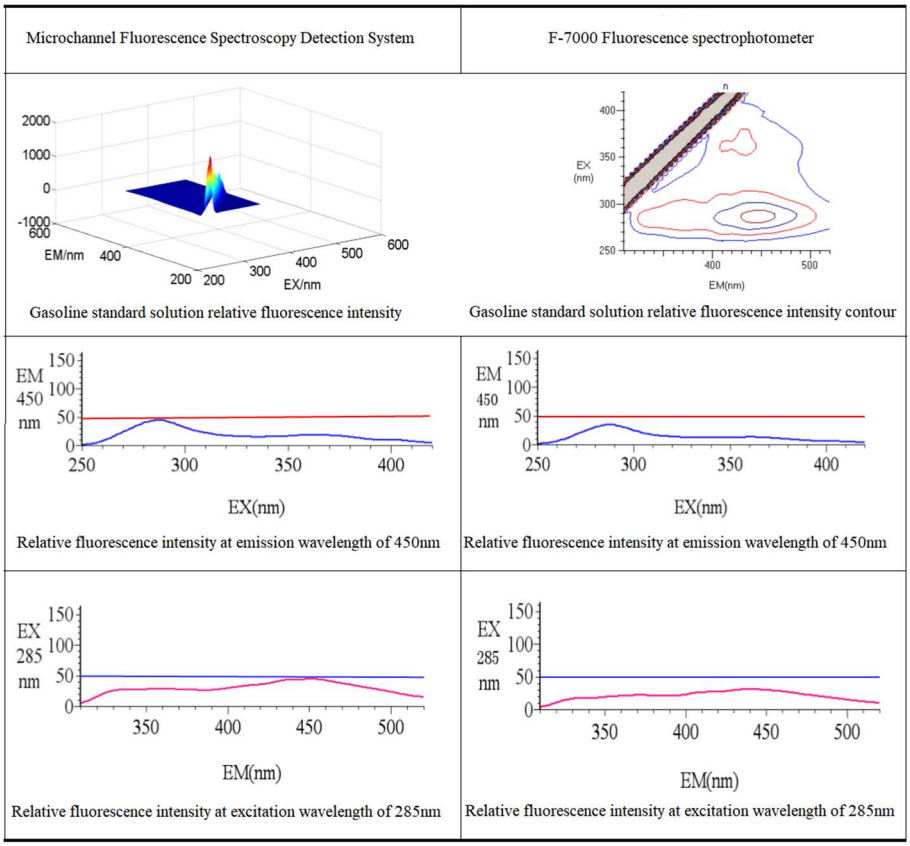

FIGURE 11. **Fluorescence spectra of gasoline standard solution.**

samples. The sample concentration is shown in Table 1. Among the three components, the samples no. 1-22 samples were used as the calibration samples, and the samples no. 23-30 samples were used as the prediction samples. The sample concentration is shown in Table 2. The excitation spectrum range of the microchannel fluorescence spectroscopy experimental system is set to 250-430 *nm*, the emission spectrum range is set to 310-520 *nm*, and the width of the entrance slit and the exit slit is 2 *mm*.

As shown in Figure 13, the three-dimensional fluorescence peak of pure sample 0#diesel oil is at 406/420 *nm*. Figure 14 is the fluorescence spectrum of 97 # gasoline CCl_4 solution. The peak is at 384/440 *nm*, and there is a slightly lower fluorescence peak at 380/434 *nm*.

The excitation-emission matrix spectra of 1-12 samples are measured. The contour fluorescence spectra of 1-12 samples are shown in Figure 15, it can be seen from the figure that three fluorescence peaks representing the corresponding three components in each sample can be easily identified.

Before the traditional parallel factor analysis, the kernel consistent diagnosis method is used to determine the component score. The relationship between the nuclear consistent value and the number of components is shown in Figure 16. After calculation, it was found that when $F \leq 10$, all three factors could not be obtained at the same time, which were consistent with the existence of the three oils in the mixed solution sample set. The excitation spectra, emission spectra and concentration loading score obtained by 10-factor parallel factor analysis are shown in Figures.17,18 and 19. As shown in Figure 19, the concentration load scores of each factor in sample 2 containing only gasoline are not equal to or close to 0, and the parallel factor model cannot explain the composition of the mixed system well. The generalized inverse singular value decomposition is used to improve the parallel factor algorithm, which does not need to determine the number of components, has high resolution and fast convergence speed.

The improved parallel factor analysis was performed on the three-dimensional fluorescence spectral matrix data of the mixed solutions of three petroleum substances. The two-dimensional spectra of the three components are obtained as shown in Figure 20. It can be seen from the figure that there is a maximum excitation intensity peak and a maximum emission intensity peak for all three components. The maximum excitation and emission wavelengths of component 1 were 380/410 nm, respectively, indicating the spectral characteristics of 97# gasoline. The maximum excitation and emission wavelengths of component 2 were 400/415 nm, respectively, indicating the spectral characteristics of 0#diese.

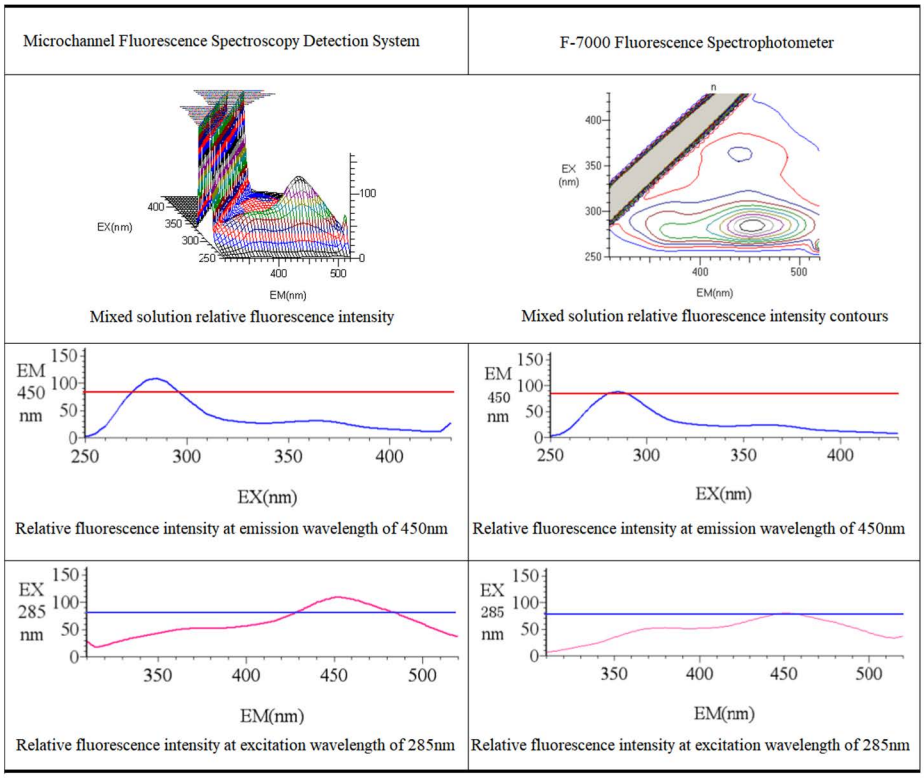

FIGURE 12. Fluorescence spectra of mixed solution.

TABLE 1. Concentration of four components samples (unit:mg/L).

Sample	-10#Diesel	97#Gasoline	93#Gasoline	Kerosene
1	40	20	20	40
2	10	50	40	20
3	60	30	70	50
4	0.8	0.5	1.0	0.7
5	1.0	0.6	0.9	0.5
6	0.2	0.5	0.2	0.4
7	0.4	0.2	0.5	0.1
8	0.7	1.0	0.2	0.6
9	40	15	30	60
10	20	30	50	10

The maximum excitation and emission wavelengths of component 3 were 280/460 nm, respectively, indicating the spectral characteristics of common kerosene. The predicted concentrations and Average recovery rate of three components in 23-30 samples obtained by improved parallel factor analysis are listed in table 3. The results show that the improved parallel factor method can not only identify the specific components of micro-content in the mixed solution samples, but also quantitatively determine the concentration of each component.

The four oils of different concentrations were mixed in CCl_4 solution, and the three-dimensional array ($43 \times 37 \times 6$) of the four-component calibration sample obtained by scanning was extracted, Among them, 43 is the number of sampling points of emission wavelength, 37 is the number of sampling points of excitation wavelength,

TABLE 2. The concentration of three components samples (unit:mg/L).

Sample	0#Diesel	97#Gasoline	Kerosene	Sample	0#Diesel	97#Gasoline	Kerosene
1	0.3	0.5	0.1	16	20	40	80
2	0	0.6	0	17	45	60	30
3	0.2	0.5	0.1	18	80	15	40
4	0.5	0.2	0.1	19	60	30	10
5	0.1	0.8	0.3	20	30	20	50
6	0.3	0.1	0.5	21	70	10	35
7	0.5	0.5	0.5	22	10	90	20
8	0.4	0.3	0.8	23	0.2	0.4	0.3
9	1.0	1.0	1.0	24	0.7	0.5	1.0
10	0.5	0.8	1.2	25	0.6	0.8	0.2
11	0.8	1.0	0.5	26	0.8	0.2	0.4
12	1.0	0.5	0.8	27	20	15	50
13	20	50	30	28	80	10	10
14	40	25	60	29	25	60	5
15	15	80	35	30	10	20	40

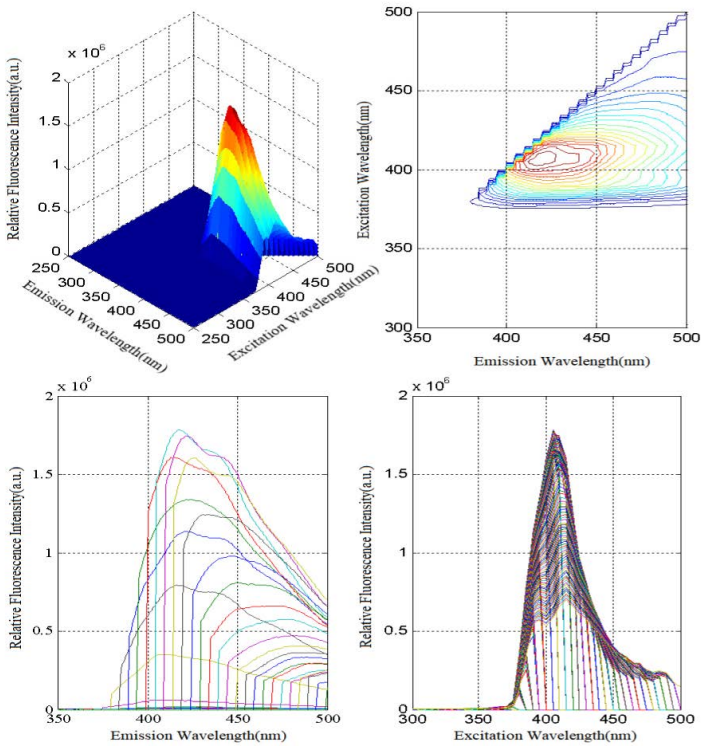

FIGURE 13. The fluorescence spectrum of pure 0# diesel sample.

and 6 is the number of calibration samples No. 1-6. The improved parallel factor algorithm was used to analyze the experimental samples, and the two-dimensional maps of four main components were obtained. The experimental analysis results of the four-component samples are shown in Figure 21.

In the four-factor analytical results, the maximum excitation wavelength and emission wavelength of component 1

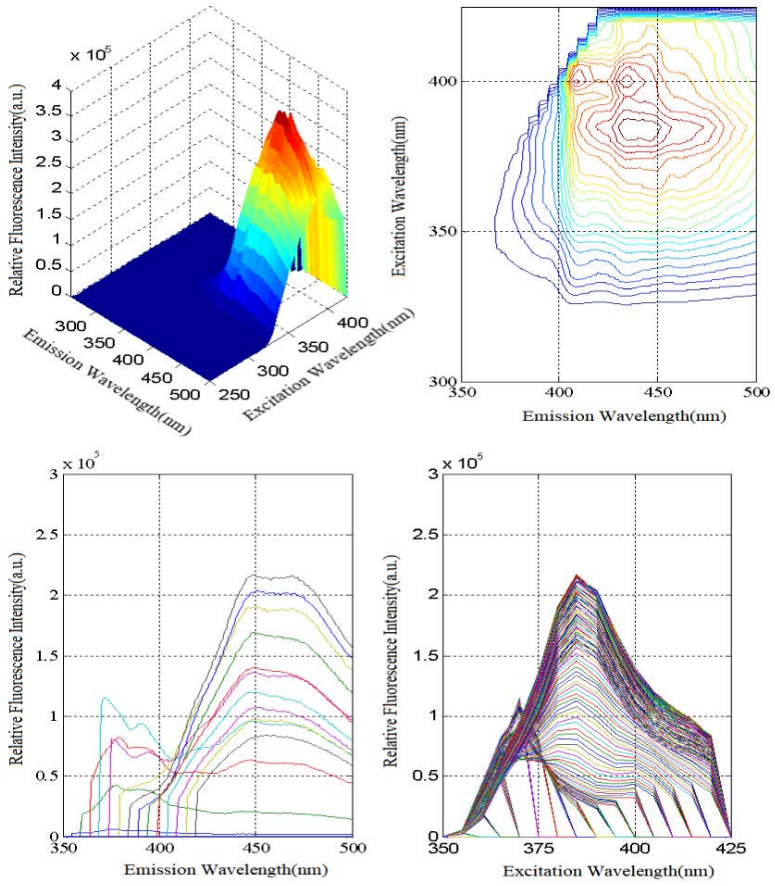

FIGURE 14. The fluorescence spectrum of 97# gasoline in CCl_4.

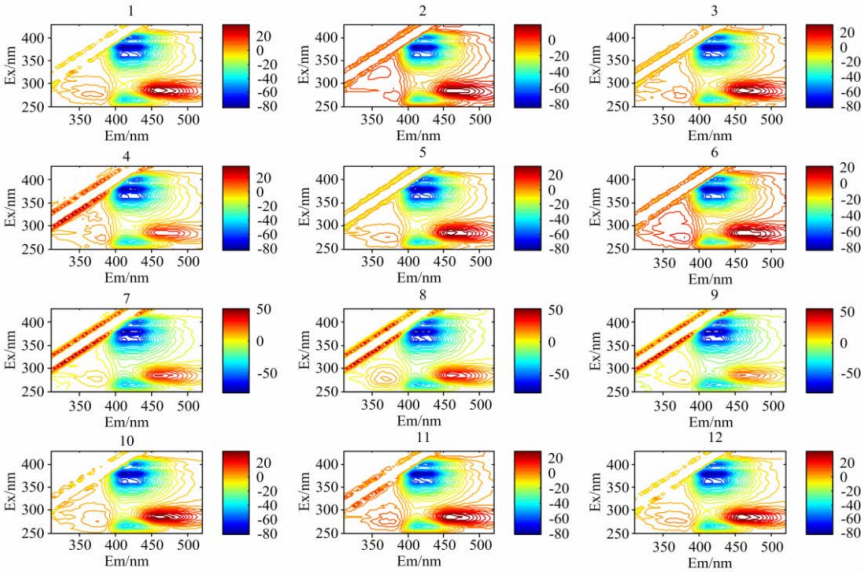

FIGURE 15. Contour fluorescence spectra of 1-12 samples.

were 285/450 nm, showing the spectral characteristics of kerosene. The maximum excitation emission wavelength of component 2 is 395/435 nm, which shows the spectral characteristics of 97# gasoline. The maximum excitation wavelength and emission wavelength of component 3 were 400/410 nm, showing the spectral characteristics of

TABLE 3. Prediction concentration and recovery rate of the three components prediction samples.

Sample	Predict concentration (mg/L)			Recovery rate (%)			Average recovery rate (%)		
	0#Diesel	97#Gasoline	Kerosene	0#Diesel	97#Gasoline	Kerosene	0#Diesel	97#Gasoline	Kerosene
23	0.235	0.373	0.326	117.50	93.25	108.67			
24	0.689	0.493	0.983	98.43	98.60	98.30			
25	0.617	0.793	0.197	102.83	99.13	98.50			
26	0.758	0.215	0.389	94.75	107.50	97.25			
27	20.07	14.21	48.32	100.85	94.73	96.64	101.03	98.55	98.95
28	78.97	9.64	9.67	98.71	96.40	96.70			
29	24.21	58.69	4.78	96.84	97.82	95.60			
30	9.83	20.19	39.97	98.30	100.95	99.93			

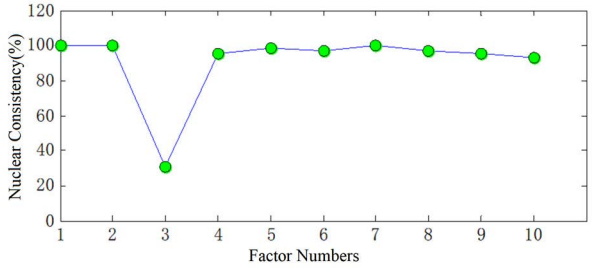

FIGURE 16. Nuclear consistency analysis results.

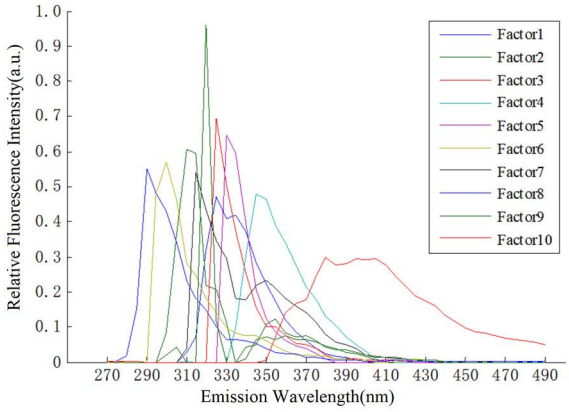

FIGURE 17. Fluorescence emission spectra of 10-factor PARAFAC analysis results.

93# gasoline. The maximum excitation emission wavelength of component 4 is 380/400 nm, which shows the spectral characteristics of −10# diesel. The aromatic hydrocarbon substances contained in 97# gasoline and 93# gasoline are similar, so their characteristic spectra are similar. But 97# gasoline will produce multiple fluorescence peaks and the fluorescence phenomenon is obvious, so component 2 is 97# gasoline, component 3 is 93# gasoline. The

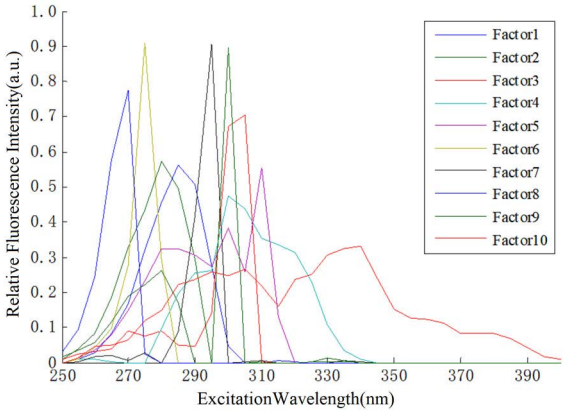

FIGURE 18. Fluorescence excitation spectra of 10-factor PARAFAC analysis results.

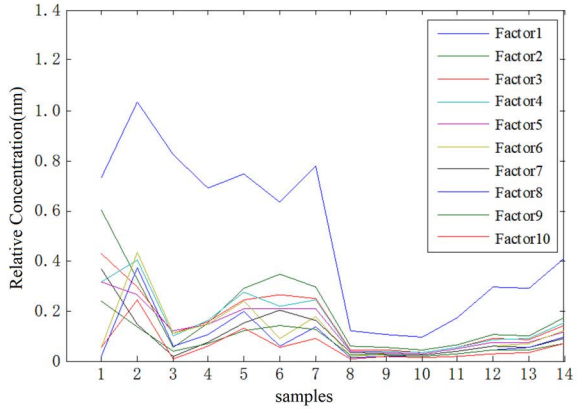

FIGURE 19. Concentration pattern of 10-factor PARAFAC analysis results.

predicted concentrations and average recovery rate of the four-component samples predicted from the predicted samples are shown in Table 4.

TABLE 4. Prediction concentration and recovery rate of the four components prediction samples.

Sample	Predict concentration (mg/L)				Average recovery rate (%)			
	0#Diesel	97#Gasoline	93#Gasoline	Kerosene	0#Diesel	97#Gasoline	93#Gasoline	Kerosene
7	0.393	0.193	0.489	0.097				
8	0.689	1.03	0.199	0.607	100.17	99.39	98.30	100.08
9	41.26	14.92	28.97	59.79				
10	20.17	29.57	49.67	10.25				

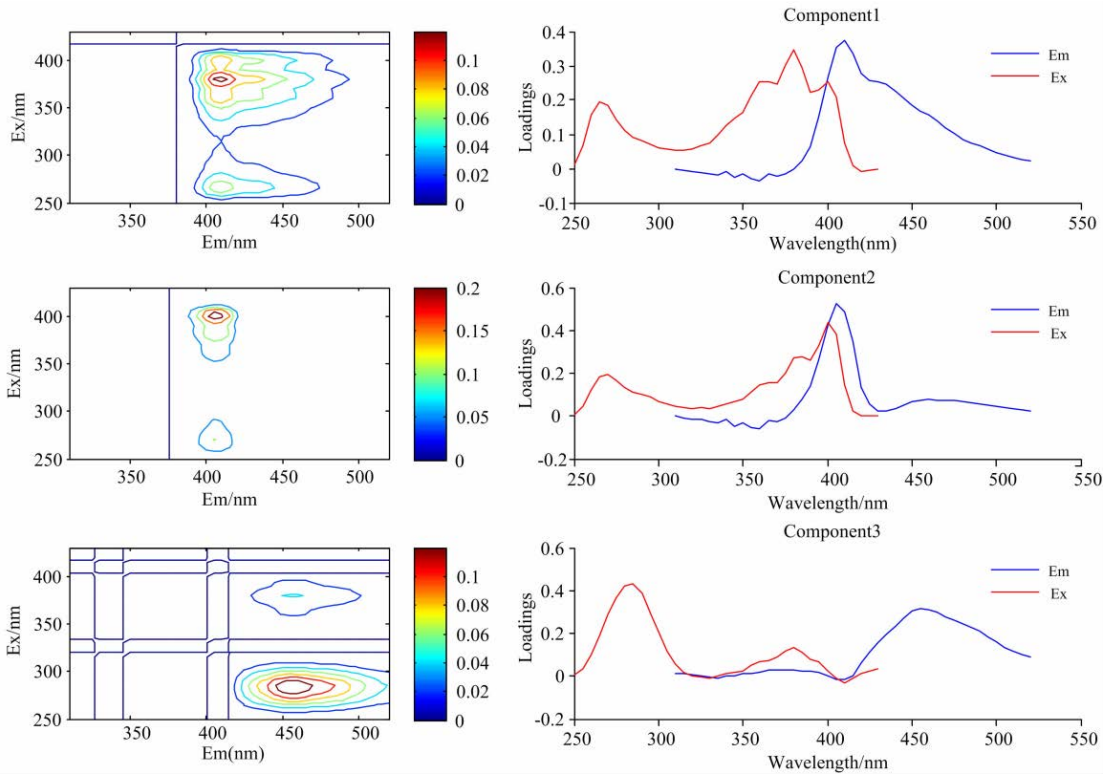

FIGURE 20. Excitation and emission spectra decomposed by improved PARAFAC.

TABLE 5. Fluorescence peak position of three oil products.

Oil types	Fluorescence peak position (Ex/Em) (nm)
97#Gasoline	390/425、410/450、430/520
0#Diesel	280/350、400/415
Kerosene	300/410、280/450、330/450、345/450

In order to verify the effectiveness and practicability of the improved method in this paper in the real environment, We collected samples from the sewage outlet of petrochemical plants, and a solution of carbon tetrachloride and oil pollutants was prepared. The ratio of the oil substance and the carbon tetrachloride was 1:1000, which was used to gradually dilute 30 samples with different concentrations. The samples no. 1-22 samples were used as the training samples, and the samples no. 23-30 samples were used as the test samples. The excitation spectrum range of the microchannel fluorescence spectroscopy experimental system is set to 230-500 nm, the emission spectrum range is set to 250-650 nm, and the width of the entrance slit and the exit slit is 2 mm.

The improved parallel factor analysis was performed on the measured samples to obtain the three-dimensional fluorescence spectra of the oil-bearing species. The fluorescence peak position of the three oils is shown in Table 5. As shown in Figure 22, 23 and 24. The maximum excitation and

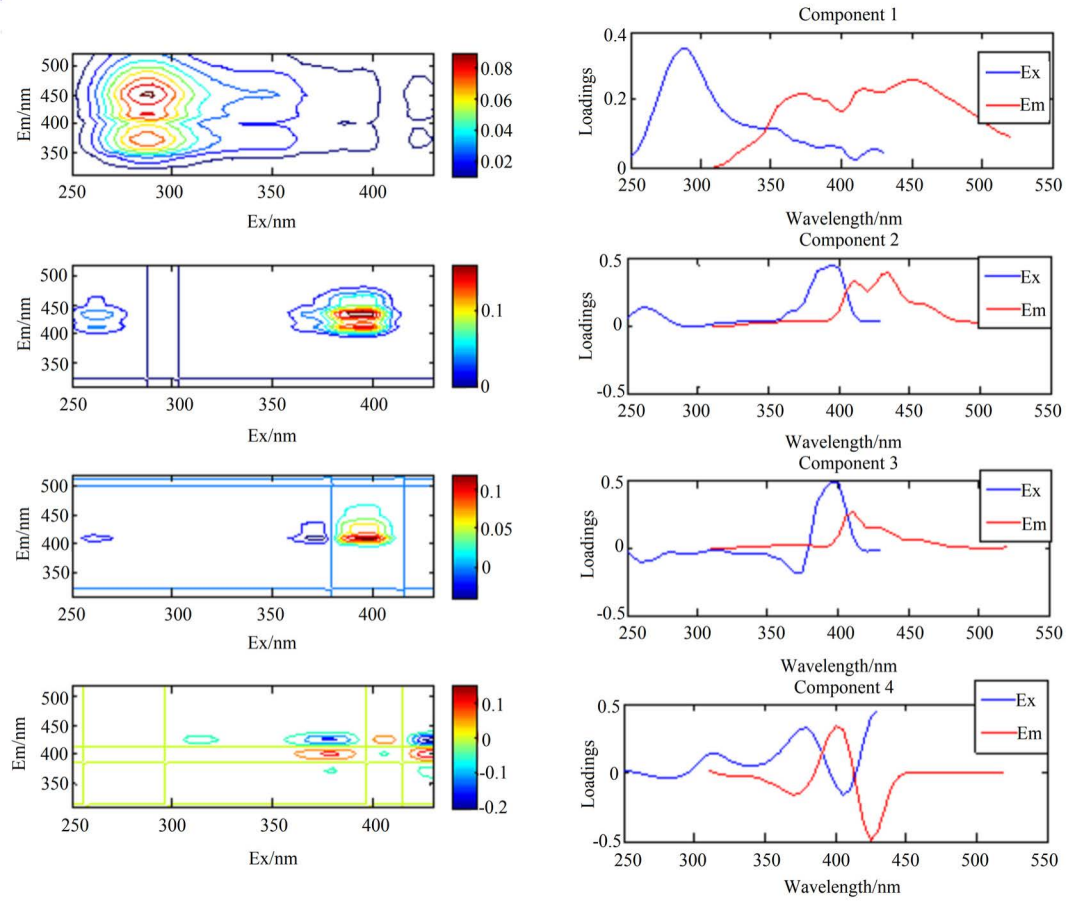

FIGURE 21. Four components spectrogram decomposed by improved PARAFAC.

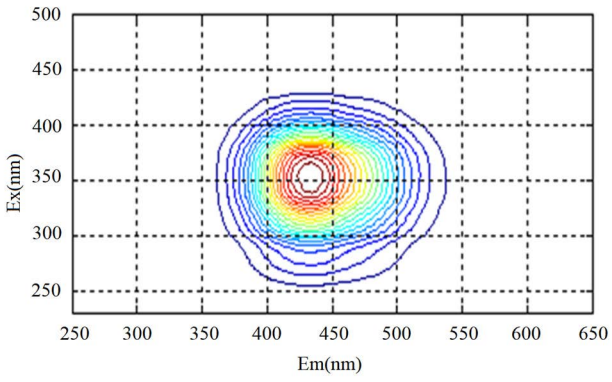

FIGURE 22. Oil pollutant component 1 contour map.

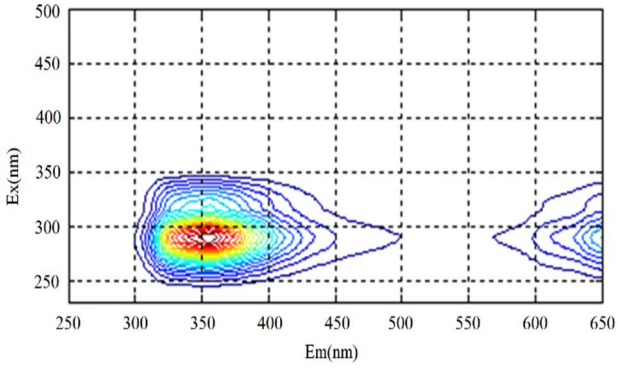

FIGURE 23. Oil pollutant component 2 contour map.

emission wavelengths of component 1 were 350/430 nm, respectively, indicating the spectral characteristics of kerosene. The maximum excitation and emission wavelengths of component 2 were 290/350 nm, respectively, indicating the spectral characteristics of 0#diese. The maximum excitation and emission wavelengths of component 3 were 450/520 and 470/520 nm, respectively, indicating the spectral characteristics of common 97# gasoline. It is verified that the three-dimensional fluorescence spectrum obtained by the analysis corresponds to the fluorescence peak range of the three oils measured in the laboratory and compared with the data measured by the water quality research center of

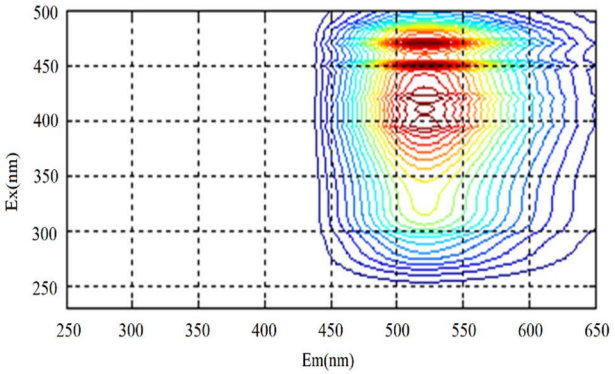

FIGURE 24. Oil pollutant component 3 contour map.

petrochemical company, the concentration error is smaller, which verified the effectiveness and accuracy of the improved parallel factor analysis method in the identification of real oil pollutants.

VI. CONCLUSION

In this paper, a fluorescence detection system with four-channel sample cell structure was developed and the grating spectrophotometer system was improved. Compared with the accuracy of traditional fluorescence spectrophotometer, the sensitivity of fluorescence detection and wavelength scanning resolution were improved. The parallel factor algorithm is improved by the generalized inverse singular value decomposition method. With the CCl_4 solution of gasoline, diesel and kerosene as the research objects, the excitation-emission matrix spectral data and three-dimensional fluorescence spectra of different samples were obtained. The improved parallel factor analysis algorithm was used to separate the fluorescence spectrum data of diesel, gasoline and kerosene mixed solution samples, and the identification of different petroleum components in the mixed solution samples was completed. The experimental results show that compared with the F-7000 fluorescence spectrometer, the improved microchannel fluorescence spectrum detection system can obtain stronger oil fluorescence signals, so as to characterize more fluorescence information, which is convenient for the qualitative and quantitative research of different oil types in the future. The improved microchannel fluorescence spectrum detection system combined with the improved parallel factor algorithm was used for the identification of three-component and four-component mixed oil. The average recoveries of 0# diesel, 97# gasoline and kerosene in the three components were 101.03%, 101.03% and 98.95%, respectively. The average recoveries of 0# diesel, 97# gasoline, 93# gasoline and kerosene in the four components were 100.17%, 99.39%, 98.30% and 100.08%, respectively, the improved microchannel laser induced fluorescence detection technology was applied to the samples collected from the sewage outlet of the petrochemical plant, which verified the effectiveness and accuracy of this method in the identification of real mixed oil components.

REFERENCES

[1] N. Idris, M. A. Gondal, K. Lahna, M. Ramli, A. M. Sari, R. K. AlDakheel, R. Mitaphonna, M. A. Dastageer, K. Kurihara, K. H. Kurniawan, and M. A. Almesserie, "Geochemistry study of soil affected catastrophically by tsunami disaster triggered by 2004 Indian ocean earthquake using a fourth harmonics (λ = 266 nm) nd:YAG laser induced breakdown spectroscopy," *Arabian J. Chem.*, vol. 15, no. 7, Jul. 2022, Art. no. 103847, doi: 10.1016/j.arabjc.2022.103847.

[2] Y. Saito, K. Ichihara, K. Morishita, K. Uchiyama, F. Kobayashi, and T. Tomida, "Remote detection of the fluorescence spectrum of natural pollens floating in the atmosphere using a laser-induced-fluorescence spectrum (LIFS) LiDAR," *Remote Sens.*, vol. 10, no. 10, pp. 1–12, Oct. 2018, doi: 10.3390/rs10101533.

[3] G. Dong, X. Li, R. Yang, Y. Yang, H. Liu, and N. Wu, "Correction method of effect of soil moisture on the fluorescence intensity of polycyclic aromatic hydrocarbons based on near-infrared diffuse reflection spectroscopy," *Environ. Pollut.*, vol. 269, Jan. 2021, Art. no. 116150, doi: 10.1016/j.envpol.2020.116150.

[4] S. Luo, C. Yan, and D. Chen, "Preliminary study on coffee type identification and coffee mixture analysis by light emitting diode induced fluorescence spectroscopy," *Food Control*, vol. 138, Aug. 2022, Art. no. 109044, doi: 10.1016/j.foodcont.2022.109044.

[5] L. Lu, S. Ichimura, T. Moriyama, A. Yamagishi, and T. Rokunohe, "A system to detect small amounts of oil leakage with oil visualization for transformers using fluorescence recognition," *IEEE Trans. Dielectr. Electr. Insul.*, vol. 24, no. 2, pp. 1249–1255, Apr. 2017, doi: 10.1109/TDEI.2017.006110.

[6] X. Zhang, B. Xie, M. Zhong, and H. Hao, "Research on the fluorescence distribution of the emulsified oil spills on the sea surface based on LIF," *Opt. Commun.*, vol. 520, Oct. 2022, Art. no. 128492, doi: 10.1016/j.optcom.2022.128492.

[7] S. D. Alaruri, "Multiwavelength laser induced fluorescence (LIF) LiDAR system for remote detection and identification of oil spills," *Optik*, vol. 181, pp. 239–245, Mar. 2019, doi: 10.1016/j.ijleo.2018.12.073.

[8] K. Bian, M. Zhou, F. Hu, W. Lai, and M. Huang, "CEEMD: A new method to identify mine water inrush based on the signal processing and laser-induced fluorescence," *IEEE Access*, vol. 8, pp. 107076–107086, 2020, doi: 10.1109/ACCESS.2020.3000333.

[9] S. Chen, X. Du, W. Zhao, P. Guo, H. Chen, Y. Jiang, and H. Wu, "Olive oil classification with laser-induced fluorescence (LIF) spectra using 1-dimensional convolutional neural network and dual convolution structure model," *Spectrochimica Acta A, Mol. Biomolecular Spectrosc.*, vol. 279, Oct. 2022, Art. no. 121418, doi: 10.1016/j.saa.2022.121418.

[10] W. R. Mohamed, N. Mahmoud, F. A. Samad, E. Ahmed, M. R. Hamblin, and T. Mohamed, "Rapid monitoring of serum albumin as a biomarker of liver and kidney diseases using femtosecond laser-induced fluorescence," *Spectrochimica Acta A, Mol. Biomolecular Spectrosc.*, vol. 268, Mar. 2022, Art. no. 120646, doi: 10.1016/j.saa.2021.120646.

[11] Y. Duan, C. Wang, X. Geng, G. Wang, and Y. Guan, "A highly sensitive optical fiber based near-infrared laser induced fluorescence detector (LIF) for parathyroid gland detection," *Sens. Actuators B, Chem.*, vol. 364, Aug. 2022, Art. no. 131879, doi: 10.1016/j.snb.2022.131879.

[12] G. Chang, X. Yu, J. Peng, Y. Yu, Z. Cao, L. Gao, M. Han, and G. Wu, "Absorption, quenching, and enhancement by tracer in acetone/toluene laser-induced fluorescence," *Chin. Phys. B*, vol. 29, no. 12, Dec. 2020, Art. no. 124212.

[13] Z. A. Duca, N. C. Speller, M. E. Cato, G. G. Morbioli, and A. M. Stockton, "A miniaturized, low-cost lens tube based laser-induced fluorescence detection system for automated microfluidic analysis of primary amines," *Talanta*, vol. 241, May 2022, Art. no. 123227, doi: 10.1016/j.talanta.2022.123227.

[14] T. Liénard–Mayor, J. S. Furter, M. Taverna, H. V. Pham, P. C. Hauser, and T. D. Mai, "Modular instrumentation for capillary electrophoresis with laser induced fluorescence detection using plug-and-play microfluidic, electrophoretic and optic modules," *Analytica Chim. Acta*, vol. 1135, pp. 47–54, Oct. 2020, doi: 10.1016/j.aca.2020.08.025.

[15] J. Huang, D. Wang, Y. Lei, Y. Wang, P. Deng, H. Cai, and J. Liu, "Measurement of energy distribution of output electrons from a microchannel plate based on vacuum photodiode," *IEEE Access*, vol. 9, pp. 144080–144084, 2021, doi: 10.1109/ACCESS.2021.3121718.

[16] J. Kim, H. Cho, J. Kim, J. S. Park, and K.-H. Han, "A disposable smart microfluidic platform integrated with on-chip flow sensors," *Biosensors Bioelectron.*, vol. 176, Mar. 2021, Art. no. 112897, doi: 10.1016/j.bios.2020.112897.

[17] Z. Li, X. Ding, K. Yin, L. Avery, E. Ballesteros, and C. Liu, "Instrument-free, CRISPR-based diagnostics of SARS-CoV-2 using self-contained microfluidic system," *Biosensors Bioelectron.*, vol. 199, Mar. 2022, Art. no. 113865, doi: 10.1016/j.bios.2021.113865.
[18] J. Li, Y. Liu, Y. Li, X. Li, J. Liang, and S. Qu, "Microfluidic volume optical monitoring system based on functional channels integrated by hollow cylindrical waveguide," *Measurement*, vol. 193, Apr. 2022, Art. no. 110951, doi: 10.1016/j.measurement.2022.110951.
[19] D. Zaremba, S. Blonski, and P. M. Korczyk, "Concentration on demand—A microfluidic system for precise adjustment of the content of single droplets," *Chem. Eng. J.*, vol. 430, Feb. 2022, Art. no. 132935, doi: 10.1016/j.cej.2021.132935.
[20] K. Mangalgiri, Z. Cheng, S. Cervantes, S. Spencer, and H. Liu, "UV-based advanced oxidation of dissolved organic matter in reverse osmosis concentrate from a potable water reuse facility: A parallel-factor (PARAFAC) analysis approach," *Water Res.*, vol. 204, Oct. 2021, Art. no. 117585, doi: 10.1016/j.watres.2021.117585.
[21] O. Rinot, M. Borisover, G. J. Levy, and G. Eshel, "Fluorescence spectroscopy: A sensitive tool for identifying land-use and climatic region effects on the characteristics of water-extractable soil organic matter," *Ecol. Indicators*, vol. 121, Feb. 2021, Art. no. 107103, doi: 10.1016/j.ecolind.2020.107103.
[22] B. Liu, J. Wu, C. Cheng, J. Tang, M. F. S. Khan, and J. Shen, "Identification of textile wastewater in water bodies by fluorescence excitation emission matrix-parallel factor analysis and high-performance size exclusion chromatography," *Chemosphere*, vol. 216, pp. 617–623, Feb. 2019, doi: 10.1016/j.chemosphere.2018.10.154.
[23] Y. Gu, Z. Zuo, C. Shi, and X. Hu, "Feasibility study for spatial distribution of diesel oil in contaminated soils by laser induced fluorescence," *Appl. Sci.*, vol. 10, no. 3, p. 1103, Feb. 2020, doi: 10.3390/app10031103.
[24] Y. Cui, D. Kong, L. Kong, S. Wang, and H. Shi, "A novel strategy for identifying oil pollutants based on excitation-emission matrix fluorescence spectroscopy and Zernike moments," *IEEE Access*, vol. 8, pp. 17999–18006, 2020, doi: 10.1109/ACCESS.2020.2967799.
[25] Q. Wu and H. Xu, "Design and development of an on-line fluorescence spectroscopy system for detection of aflatoxin in pistachio nuts," *Postharvest Biol. Technol.*, vol. 159, Jan. 2020, Art. no. 111016, doi: 10.1016/j.postharvbio.2019.111016.
[26] Y.-Y. Yuan, S.-T. Wang, Q. Cheng, D.-M. Kong, and X.-G. Che, "Simultaneous determination of carbendazim and chlorothalonil pesticide residues in peanut oil using excitation-emission matrix fluorescence coupled with three-way calibration method," *Spectrochimica Acta A, Mol. Biomolecular Spectrosc.*, vol. 220, Sep. 2019, Art. no. 117088, doi: 10.1016/j.saa.2019.04.080.
[27] J. Sun, Y. Ren, J. Ji, Y. Guo, and X. Sun, "A novel concentration gradient microfluidic chip for high-throughput antibiotic susceptibility testing of bacteria," *Anal. Bioanal. Chem.*, vol. 413, no. 4, pp. 1127–1136, Jan. 2021, doi: 10.1007/s00216-020-03076-8.
[28] S. Höving, D. Janasek, and P. Novo, "Flow rate independent gradient generator and application in microfluidic free-flow electrophoresis," *Analytica Chim. Acta*, vol. 1044, pp. 77–85, Dec. 2018, doi: 10.1016/j.aca.2018.04.066.
[29] J. Park, H. Choi, G. Lim, D.-K. Lee, N.-C. Park, and W.-C. Kim, "Development of a wide-width raster scanning optical system for high-resolution ultraviolet laser direct micro-patterning," *Opt. Lasers Eng.*, vol. 134, Nov. 2020, Art. no. 106179, doi: 10.1016/j.optlaseng.2020.106179.
[30] M. J. M. Wells, J. Hooper, G. A. Mullins, and K. Y. Bell, "Development of a fluorescence EEM-PARAFAC model for potable water reuse monitoring: Implications for inter-component protein–fulvic–humic interactions," *Sci. Total Environ.*, vol. 820, May 2022, Art. no. 153070, doi: 10.1016/j.scitotenv.2022.153070.
[31] Y. Hu, H.-L. Wu, X.-L. Yin, H.-W. Gu, Z. Liu, R. Xiao, L.-X. Xie, H. Fang, and R.-Q. Yu, "A flexible and novel strategy of alternating trilinear decomposition method coupled with two-dimensional linear discriminant analysis for three-way chemical data analysis: Characterization and classification," *Analytica Chim. Acta*, vol. 1021, pp. 28–40, Aug. 2018, doi: 10.1016/j.aca.2018.03.050.
[32] W.-J. Long, H.-L. Wu, T. Wang, M.-Y. Dong, and R.-Q. Yu, "Interference-free analysis of multi-class preservatives in cosmetic products using alternating trilinear decomposition modeling of liquid chromatography diode array detection data," *Microchem. J.*, vol. 162, Mar. 2021, Art. no. 105847, doi: 10.1016/j.microc.2020.105847.
[33] Y. Park, S. A. MacIsaac, P. Kaur, M. Brophy, and G. A. Gagnon, "Monitoring the influence of wastewater effluent on a small drinking water system using EEM fluorescence spectroscopy coupled with a PARAFAC and PCA statistical approach," *Environ. Sci., Processes Impacts*, vol. 23, no. 6, pp. 880–889, Jun. 2021, doi: 10.1039/d1em00015b.

PENGFEI CHENG was born in Shandong, China, in 1986. He received the B.S. degree in measurement and control technology and instrument specialty from Hebei University of Engineering, Hebei, China, in 2011, and the Ph.D. degree in instrument science and technology from Yanshan University, Hebei, in 2017. He is currently a Lecturer with the School of Electrical and Control Engineering, Xuzhou University of Technology. His research interests include fluorescence spectrum detection technology and photoelectric detection and image processing technology.

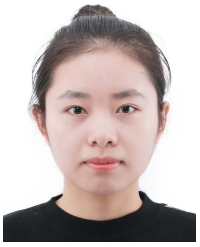

YANPING ZHU was born in Shandong, China, in 1997. She received the B.S. degree in electrical engineering and automation from Linyi University, Shandong, in 2020. She is currently pursuing the M.S. degree in instrument science and technology with the North China University of Science and Technology, Hebei, China. Her research interests include fluorescence spectrum detection technology and photoelectric detection and image processing technology.

CHUANJIN CUI was born in Shandong, China, in 1982. He received the B.S. degree in agricultural mechanization and automation from Tianjin Agricultural University, Tianjin, China, in 2006, and the Ph.D. degree in agricultural mechanization engineering from Shanxi Agricultural University, Shanxi, China, in 2011. He was a Visiting Scholar at the University of Ottawa, Canada, from 2016 to 2017. He is currently an Adjunct Professor with the College of Electrical Engineering, North China University of Science and Technology, Hebei. His research interests include biosensor technology, analytical testing technology, and intelligent instrument.

JINYAN PAN was born in Hebei, China, in 1987. She received the B.S. degree in measurement and control technology and instrument and the M.S. degree in instrument science and technology from Yanshan University, Hebei, in 2011 and 2014, respectively. She is currently a Lecturer with the School of Electrical and Control Engineering, Xuzhou University of Technology. Her research interests include fluorescence spectrum detection technology and photoelectric detection and image processing technology.